Proceedings of the 2017 IEEE
International Conference on Robotics and Biomimetics
December 5-8, 2017, Macau SAR, China

A Kalman filter based force-feedback control system for hydrodynamic investigation of unsteady aquatic propulsion

Tao Yuan, Ziyu Ren, Kainan Hu, Mengxi Ren, Siqi Wang, Tianmiao Wang, **Li Wen***

Abstract—**Recent advances in understanding fish locomotion with robotic devices have included the use of different robotic prototypes that swim at a controlled but constant swimming speeds. However, the speed of even steadily swimming live fishes is not constant because the fish commonly accelerate and decelerate throughout tail beat cycles. In this paper, we implement a bass body-shaped robot, programmed to display the carangiform fish locomotion. The robotic fish was then mounted on a servo towing system and initially at rest, can determine its self-propelled speed by measuring the external force acting upon it. A Kalman filter was used for filtering the measured external force. By using this method, we tested the speed profiles of both a customized ROV and the robotic fish model. The results show that this experimental method can well predict the speed profiles of both the traditional propeller-based and the undulatory robotic swimmers. In particular, we show that the linear acceleration phase can be reproduced by this experimental method. Finally, we discuss this force-feedback-controlled method and the relative self-propelled hydrodynamic results of the robot.**

I. INTRODUCTION

Compared with the man-made underwater vehicles, fish possess excellent swimming performance with high efficiency and maneuverability, which let fish become the source of many inspirations for engineers to produce alternative designs [1][2]. In the past few decades, a series of robotic fish prototypes have been developed. They can be roughly divided into two categories: the ones that aim to swim in the open water for engineering implementation [3][4] and the ones that are tethered to a rail system or the ground fixtures, aiming for fundamental biomechanics research [5][6]. Quantitatively measuring the swimming performance of the robotic fish has important significance for understanding the principle behind the fish-like propulsion and for engineering applications.

However, restricted by the limited loading space due to the tapered body, the free-swimming robotic fish is hard to carry sufficient equipment for hydrodynamic experiments underwater. Most of the hydrodynamic investigations are conducted on the robotic prototypes that have greater carrying capability and are more similar to the biological counterparts, while, can only be fixed to the ground or propel along a rail. On the other hand, the oversimplified morphology and the movement pattern also limit their application in understanding the propulsion principles of the fish-like swimming. There are mainly two methods to test the swimming performance on these constraint-swimming robotic models. The first method, as shown in Fig.1A, is called the active-towing method [7]. The prototype is mounted on a towing system and towed in still water, or is fixed to the ground and submerged in a circulation water channel [8]. In this method, the towing system or the water channel can provide the prototype with a programmed

speed relative to the still water, forcing the robotic fish to "swim" at a constant velocity. However, this method dissatisfies the self-propulsion principle, which states that all the thrust force generated by the fish-like swimming motion should compensate all the drag force produced by the undulatory body during the steady swimming state, and no external force in the axial thrust direction should be exist.

The previous study has already shown that the force under the self-propelled condition is very different from that under constrained-propulsion [9]. Besides, since the speed is constant, the experiment cannot be applied to study the process when the velocity varies, such as the burst & coast [10] and the linear acceleration [11]. An alternative approach, as shown in Fig.1B, is called the passive-towing method. The robotic swimmer is connected to a low-resistance slide rail. The thrust generated by the robotic fish can propel the fish and the experiment equipment along the towing system. This method ensures the robotic fish is swimming under the self-propulsion condition. However, the additional mass of the equipment added onto and significantly increase the "actual" mass of the prototype. The acceleration speed will be untrue under this situation, providing the fish-like movement generate equivalent thrust force. Therefore, this method is only suitable for the physical models with low mass, such as a flexible plastic foils [12][13] or a simplified light-weight robotic fish model [14].
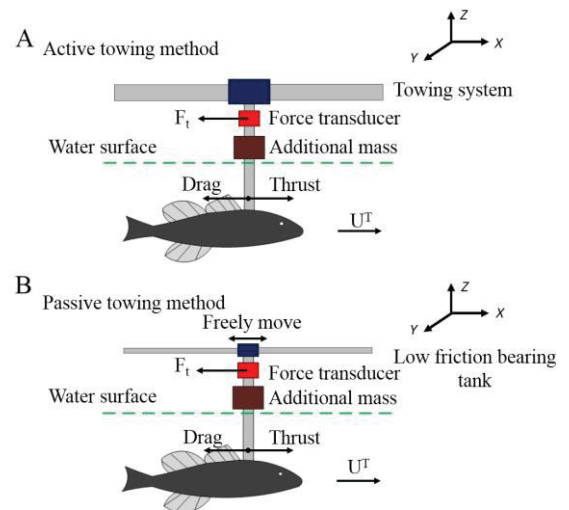

Fig.1.Schematic view of the traditional experimental setups and methods used in hydrodynamic experiments.

However, little efforts have been made to develop an experiment method under self-propulsion principle that can

The authors are with the School of Mechanical Engineering and Automation, Beihang University, Beijing, 100191, People's Republic of China;
* E-mail for contact: liwen@buaa.edu.cn

make up for the defects in traditional methods. The hydrodynamic flow field under constraint-propulsion state is very different from that under self-propulsion state [9]. In recent years, increasing studies have been performed through CFD simulations that satisfy self-propulsion principles to reveal the fish-like swimming mechanisms [15][16]. In this paper, we presented a self-propulsion method based on our previous work [17][18] for experiments on robotic fish. Details about the hardware devices and the control algorithm are introduced. We used a remotely-operated vehicle (ROV) and a multi-joint robotic fish to verify the effectiveness of the experiment method to measure the propulsion velocity of both propeller-based swimmer and fish-like swimmer. We compared the velocity profiles of two kinds of swimmers to demonstrate the necessity to apply the self-propulsion method in experiments on physical models, especially for robotic fish experiments.

II. MATERIALS AND METHODS
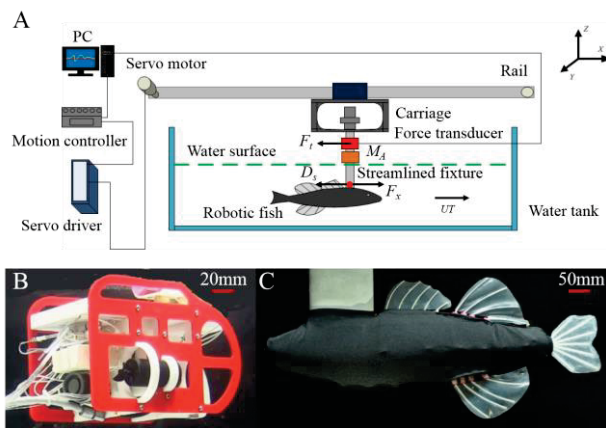
A. Experiment Device

Fig.2. Experiment apparatus. (A) Schematic of the experiment system. (B) The ROV used to verify our control system. (C) The robotic fish used to investigate the unsteady swimming.

The experiment platform of the force-feedback control system is shown in Fig.2A, it mainly includes a set of servo towing system that can move in the x direction. The servo towing system has a travel distance of 7.5 m with a position control accuracy of 0.1 mm. There is a water tank measuring 7.8m × 1.2m × 1.1m underneath the towing system, in which the robotic fish has sufficient space to move. Besides, in order to avoid the interference effect of the water surface and the tank bottom, the robotic model was mounted at mid-depth in the tank. The robotic swimmer was fixed below the force sensor by a streamlined fixture to reduce the flow resistance generated during swimming. The external force of a robotic swimmer can be measured using a multi-axis ATI force transducer (mini-40, ATI Industrial Inc., Canada).The force data collected was then sent to a computer to calculate the speed of robotic swimmer in real time.

Underwater robotic swimmer used in the experiment includes a propeller-driven ROV and a bionic robotic fish. The ROV shown in Fig.2B was used to demonstrate the effectiveness of the Kalman filter based force-feedback control

system in propeller-based propulsion. The ROV was driven by two 300W DC motors, which can be controlled by a motor speed controller. The weight of the ROV is 1.46 kg and its length, width and height are 220mm, 140mm and 160mm respectively. The bionic robotic fish we used, shown in Fig.2C, was aim to verify the effectiveness of the control system in unsteady swimming. It has a total length of 588 mm and 2.79 kg and a very similar shape to a carangiform fish with four individual body segments. The posterior segment can rotate relative to the previous one. The power of each body segment was provided by a servo motor (RE40, Maxon Motor Inc., Switzerland),which was mounted above the water surface, and was transmitted through a belt-transmitting mechanism. The motion control of each servo motor was realized through a servo-motor movement controller (MC206, TrioMotion Technology, UK). The frequency, amplitude and the swimming mode can be freely adjusted to meet the experiment requirement. The readers can refer to our previous studies [17][18] for more details about the robotic fish.

B. Self-propelled Control method

In Fig.2A, Fx is the resultant force produced by the robotic fish along the X direction:

$$Fx = Thrust - Drag \qquad (1)$$

Ds is the fluid resistance of the streamlined fixture between the robotic fish and the sliding block. Since the streamlined fixture used in our experiments has an airfoil cross section, the magnitude of the fluid resistance is much smaller than the resultant force Fx, so it can be roughly ignored. UT is the speed provided by the towing system at the moment T. M_A is the mass of the equipment that moves with the robotic fish other than the mass of the robotic fish, which we define as the additional mass. Ft is the force applied by the towing system, which is inverse to the force measured by the force transducer directly. When the robotic swimmer is undergoing the "self-propelled" state, the force Ft applied to the robotic swimmer should be strictly 0 at every moment. However, such requirement is too harsh to current engineering implementation. To relax the "self-propelled" conditions for engineering implementation, we re-defined the "self-propelled" state according to the average force during a certain time period. That is, when average the force measured by the force transducer in one movement period (for unsteady propulsion of the robotic fish) or a fixed time period (for propeller-based propulsion of the ROV) is equal to zero, the robotic swimmer is considered to be "self-propelled". Our control algorithm was designed to accomplish this goal. We will show through experiments that this control algorithm performed pretty well under some conditions.
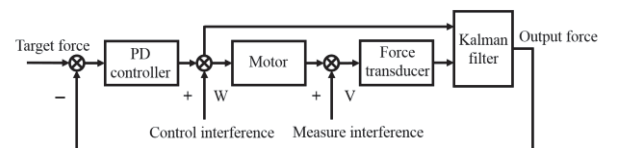

Fig.3. The block diagram of the Kalman filter based force-feedback control system. The measured force was pre-processed by Kalman filter, and was then sent to the PD controller to process. As the motor controlled the speed according to the change of error between target force and the force output, our

1215

control system would achieve "self-propelled" condition when the error approximates 0N.

Since the "self-propelled" system has strict requirements for dynamic response performance, a PD controller was designed to control the towing system. The block diagram of the control system is shown in Fig.3. The PD controller in our control system can be formulated as:

$$u(t) = K_p \left[e(t) + T_d \frac{de(t)}{dt} \right] \quad (2)$$

Where, $u(t)$ is the output of the controller, $e(t)$ is the input of the controller, and K_p, T_d are the proportional amplification coefficients and differential time of the controller respectively. In our study, the measurement of the force transducer Ft was set as the input of the controller, and the change in drag velocity ΔU was chosen as the output quantity. $\Delta U(T)$ is the output value of the controller at the sampling time T, so we can obtain the discrete expression of the PD controller:

$$\Delta U(T) = K_p \Delta F_m(T) + K_d [\Delta F_m(T) - \Delta F_m(T-1)] \quad (3)$$

$$\Delta F_m(T) = F_m(T) - F_m(T-1) \quad (4)$$

In equation (2), K_p is the proportional amplifier coefficient, $K_d = \frac{K_p T_d}{T}$ is the differential coefficient. Therefore, the motor speed of towing system at time T should be:

$$U(T) = U(T-1) + \Delta U(T) \quad (5)$$

The oscillation of the mechanical system is unavoidable and unpredictable, which is detrimental to force acquisition and seriously affect the stability of the control system. Therefore, we designed a Kalman filter to pre-process the force signal before sending back to the PD controller [20] as shown in Fig.4. The Kalman filter model can be expressed as,

System description:

$$X(k) = X(k-1) + U(k) + W(k) \quad (6)$$

$$Z(k) = H X(k) + V(k) \quad (7)$$

Optimized output process:

$$\begin{cases} X(k|k-1) = X(k-1|k-1) + U(k) \\ P(k|k-1) = P(k-1|k-1) + Q \\ X(k|k) = X(k|k-1) + Kg(k) (Z(k) - H X(k|k-1)) \\ Kg(k) = P(k|k-1) H' / (H P(k|k-1) H' + R) \\ P(k|k) = (I - Kg(k) H) P(k|k-1) \end{cases} \quad (8)$$

Where, $X(k)$ is the system state quantity, $U(k)$ is control quantity, $Z(k)$ is the observation quantity, $W(k)$ is the process noise, $V(k)$ is the measurement noise, Q and R are the covariance of the noise W, V; Kg is Kalman gain and P is covariance prediction.

We combined the general Kalman filter with the PD controller to implement the force-feedback system control, therefore, the whole control system had totally four control parameters to be adjusted. When the response of the control system was slow, we would correspondingly increase the amplification in the proportionality element of PD controller (K_p) to help speed up the system response. Note that the overlarge K_p would result in overshoot and produce oscillation, which maybe bring influence to stability. The derivative element (K_d) can predict the changing tendency of the input signal and produce effective early correction signal to increase the system's damping degree, thus improving the stability of the system. Q and R can be regarded as manually tuned parameters of Kalman filter because we obtained the values of them by adjusting. For example, if R was too small and tended to be zero, the Kalman filter would be very weak. At this time, especially the robotic fish could produce more severe shock, the oscillation would be generated when the robotic swimmer started swimming. While the value of R was too large, the speed of the robotic would be greatly reduced, even though the movement of the robotic swimmer may become smooth. As for the covariance Q, we need to make a balance between time lag and uncertainties of control system according to actual condition. Adjusting those four parameters comprehensively, the robotic swimmer achieve self-propelled with the help of the force-feedback control system.
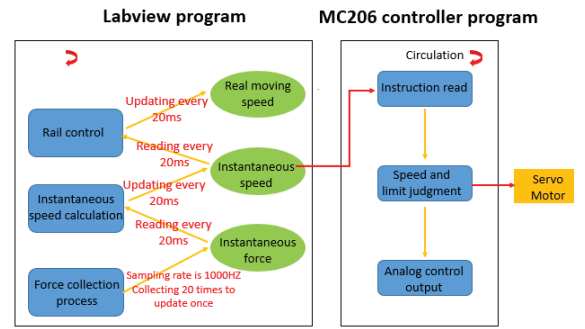

Fig.4. Flow chart of the Kalman filter based force-feedback control system.

Fig.4 is the flow chart of our control system. The upper computer program has three separate lightweight processes, which are used for force acquisition, real-time speed calculation and speed control respectively. The force acquisition program will collect force data with 1000Hz sampling rate, and then the force data will be stored in a global variable that speed calculation program can visit. The real-time speed calculation program read 20 force data from the global variable which store force data every 20ms. We will average every 20 force data to filter the force signal, and then the real-time speed calculation program will calculate the instantaneous speed of rail using the average force to reduce the fluctuation of instantaneous speed. The speed data will also be stored in a variable that rail control program can visit. The rail control program will send a speed control instruction to the MC206 controller every 20ms. The MC206 decodes the instruction and then control the speed of the motor. The algorithm of the control system was achieved through Labview (Labview2012, National Instruments, USA).

III. RESULTS

A. Speed measurement of the Propeller-based Swimmer

We compared the free swimming speed of the ROV and the speed provided by the towing system to show that the control method presented in this paper is qualified to replicate

the real propulsion process of the robotic swimmer. We obtained the free swimming speed of the ROV by a high-speed camera, which was mounted on a sliding block on the towing rail that can move together with the ROV along the *x* direction below the water surface to record the movement from the top view. The frame rate of the camera was set to 150 Hz. Since the top view camera moved relative to the ground, we used a ruler placed on the tank bottom to measure the ROV displacement. The speed of the ROV was then calculated by reading the displacement every 10 frames.
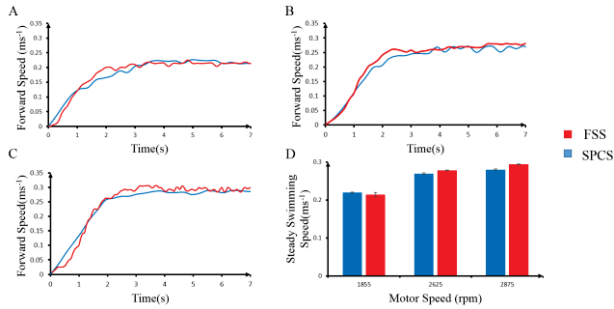

Fig.5.Comparison of the instantaneous speed profiles in free-swimming and self-propelled-control states at different motor speed: (A) 1855 RPM; (B) 2625 RPM; (C) 2870 RPM. (D) Steady swimming speed compared at different motor speed.

The velocity of the ROV was measured at three motor speed both in free-swimming state (FSS) and self-propelled-control states (SPCS). The measurement at each motor speed was repeated three times. The speed profiles in Fig.5A-C are averaged from the data obtained from three trials. The parameters of the control system are (K_p=6, K_d=0.8, Q=0.01, R=5) found through the method introduced in section 2. The velocity profiles measured in FSS and SPCS are very close, especially at low propulsion velocity (see Fig.5). When the motor speed was set to 1855 revolutions per minute (RPM), the ROV spent about 3.51s to reach the steady swimming speed which was around 0.214m/s. When ROV was in SPCS, the ROV spent about 3.67s to accelerate from still to self-propelled speed (SPS) (0.219m/s). The time of the acceleration period was 4.5% longer and the SPS was 2.3% larger than that in FSS. When the motor speed increased to 2625 RPM, however, the following error increased. The ROV took about 2.51s to swim to the steady swimming speed (0.278m/s). When the ROV was in SPCS, the ROV took about 3.17s to swim to SPS (0.269m/s). The time of the acceleration period became 26.3% longer and the SPS was 3.2% lower than that in FSS. When the motor speed reached 2870 RPM, the following error became even bigger. The ROV spent about 2.42s to reach the steady swimming speed which was around 0.0.294m/s. When ROV was in SPCS, the ROV spent about 3.08s to accelerate from still to SPS (0.280m/s). The time of the acceleration period was 27.3% longer and the SPS was 4.7% lower than that in FSS.

Fig.6 shows the axial force and the forward speed of ROV at motor speed of 2870 RPM over 8s under condition of SPCS. The integral force of every two seconds is calculated. The speed profile fluctuates around 0, which satisfies the "self-propelled" condition defined in preceding text. The maximum value of the integral is less than one percent of the force peak,

which we think the mean axial force is approximately zero. Therefore, the robotic swimmer can be considered to be at "self-propelled" condition.
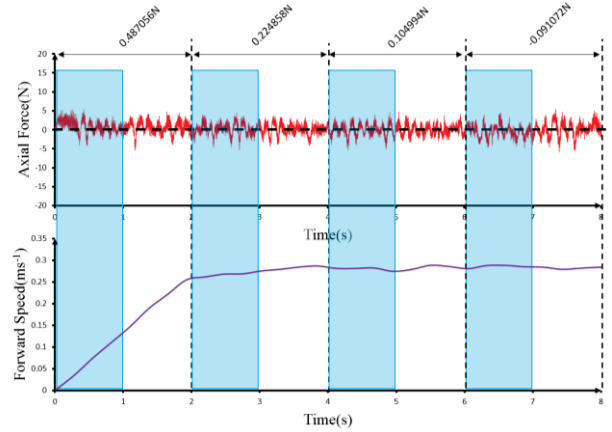

Fig.6. Instantaneous force and velocity profile at motor speed of 2870 RPM.

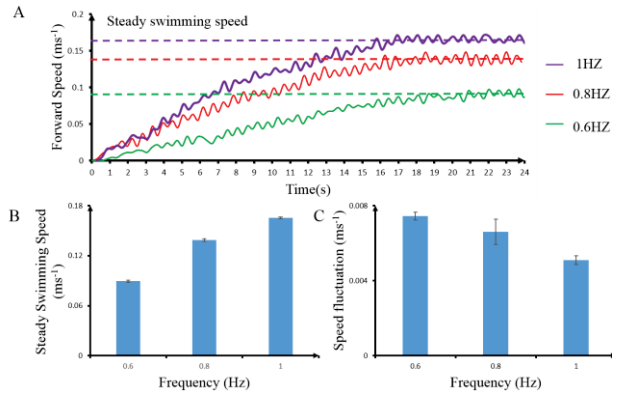## B. Speed measurement of unsteady-propelled swimmer

Fig.7. (A) Speed curves of the robotic fish at different frequencies when in SPCS. The movement process of the robotic fish can be divided into two stages, which are the acceleration stage and the steady swimming stage. (B) Steady swimming speeds at different motion frequencies. (C)Speed fluctuations at different motion frequencies.

One of the most prominent unsteady propulsion is fish swimming. In this study, we used an undulating robotic fish to mimic the unsteady-propulsion swimmer in nature. We measured the forward speed of the robotic fish at three frequency (f=0.6Hz, 0.8Hz and 1Hz) with the same undulating amplitude (0.1BL) by "self-propelled-control" method. The speed measurement was repeated three times at each frequency. The results are shown in Fig.7. The shape of the speed profiles at different motion frequency are basically similar. The robotic fish can accelerate to SPS at distinct accelerations with speed fluctuations. At motion frequency of 0.6Hz, the robotic fish accelerated for 20.35s to SPS (see the green profile in Fig.7A). When the motion frequency increased to 0.8Hz, the acceleration period was reduced to 16.82s.When the frequency was further boosted to 1Hz, the robotic fish swam significantly

faster than the other two frequencies. Fig.7B shows the mean speed of robotic fish during steady swimming state. The robotic fish with 1Hz flap frequency and 0.1 BL undulating amplitude reached the highest SPS. The 1HZ flapping pattern was 19.4% faster than the 0.8Hz condition, and 86.5% faster than the 0.6Hz condition. We also calculated the speed fluctuations (ΔV) in the axial direction, which are averaged from the absolute value of speed peak (Vp) or valley value (Vv) minus mean speed (Vm) during steady swimming state. It can be expressed by the following equation:

$$\Delta V = \frac{\left[\sum_{i=1}^{n}(|Vp_i - Vm|) + \sum_{j=1}^{n}(|Vv_j - Vm|)\right]}{2*n} \quad (9)$$

As Fig.7C shows, the 0.6Hz flapping fish body produced the maximum velocity fluctuation, with a speed fluctuation value of 0.0074 m/s during steady swimming. The 1Hz flap frequency had smaller fluctuations of 0.0051 m/s, and the 0.8Hz flap frequency had the fluctuations of 0.0066 m/s.

The instantaneous axial force and the speed profile at 0.1BL, 1Hz are shown in Fig.8. Obviously, two force peaks can be observed in each flapping cycle. Notably, the peak of the speed profile appears at the time when the peak of the force profile comes. This matches with the fish propulsion theory pretty well. We calculated the integral of every three cycles of the axial force. The maximum average axial force over three cycles of robotic fish movement was 0.307413N and mean axial force gradually reduced close to 0N.Which demonstrated that the robotic fish satisfied the self-propelled condition while swimming
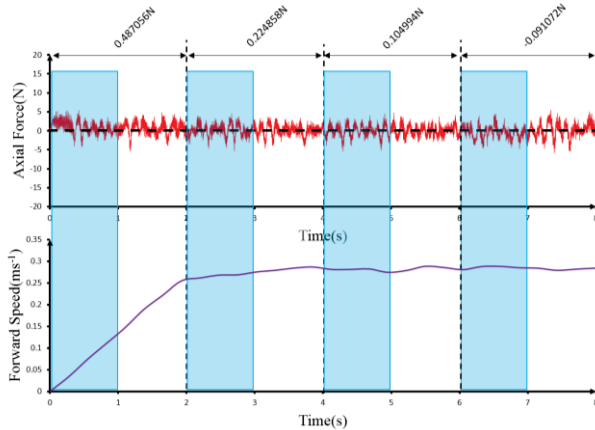

Fig.8. Force and velocity detail comparison in the case of a robotic fish movement parameter is 0.1BL/1HZ.

IV. DISCUSSION

A. The Effectiveness of the Self-propulsion Method

As mentioned earlier, when the average external force applied to the robotic swimmer by towing rail in one movement period or a fixed time period equaled to zero, the robotic swimmer was then considered to be "self-propelled". Indeed, when the external force measured by force transducer is approximate zero, the speed curve of ROV in SPCS state can basically match the speed curve of ROV in FSS. These

experiments demonstrate that the robotic swimmer would swim like free swimming under self-propelled-control system if the real-time external force was approximate 0N. There is an interesting discovery that the error between the speed curve of ROV in SPCS and that of ROV in FSS decreased when the average of real-time force was closer to zero. It reminds us that our control system can help some robotic swimmers, whose free swimming speed can't be obtained directly, such as the robotic fish whose head is fixed to the ground or propel along a rail, to achieve "self-propelled" to simulate free swimming. We can also capture the "self-propelled" speed curve, which is helpful for us to analysis the free swimming process of robotic swimmer approximately. In other words, using this test method, plenty of questions about other complicated aquatic locomotion (like C-start and burst and coast) can be answered. For example, we could try to figure out how fish median fins effect hydrodynamic force during linear acceleration. Compared with the traditional drag method, the current self-propelled-control method has two following advantages: (1) the amount of experiments that searching for self-propelled speed can be greatly reduced. Over 600 experiments were conducted on robotic tuna at fixed towing speed [19]. (2) The self-propelled-control method can obtain the unsteady swimming velocity curve contour, so that we can get motion parameters directly, such as steady swimming speed, speed fluctuation, etc. It is very useful for us to understand the whole process of robotic swimmer from the beginning to the end.

B. Difference between Fish-like Swimmer and Propeller-based Swimmer

There exists some significant differences in swimming movement process between fish-like swimmer and propeller-based swimmer: one is undulating its body, the other is using propeller. Our study may be the first quantitative investigation of speed fluctuation by self-propelled-control method. We find that the propulsion velocity curve of the fish-like swimmer obtained by self-propelled-control method was fluctuating, which is consistent with the velocity curve of CFD simulation result [15]. However, there is little speed fluctuation observed in the movement process of propeller-based swimmer in SPCS. This phenomenon is mainly caused by the fluctuation of force that was generated during robotic swimmer swimming. The force fluctuation of fish-like swimmer is almost twice that of propeller swimmer. This discover reveal that our control system has a good response performance in following real-time force change. Besides, the speed of the fish-like swimmer fluctuations cannot be captured when we used the traditional hydrodynamic investigation methods (such as the robotic fish swam at a constant speed in circulating water tank [8]). Therefore, it suggests that our study conducted to develop an experiment method following self-propulsion principles to reveal the fish-like swimming mechanisms in natural conditions is very valuable. It is necessary for people to apply the self-propulsion method in hydrodynamic experiments on physical models [22][23], especially for robotic fish experiments. In addition, comparing the velocity profiles of fish-like swimmer at different motion frequencies, we discover that the fish-like swimmer can get higher steady swimming

1218

speed at higher frequencies, which is similar to the CFD simulation of Borazjani, et al [15]. Besides, the velocity curve is smoother with small speed fluctuation when fish-like robotic fish at high frequency. This phenomenon suggests that the smaller centroid oscillation of robotic fish may be generated when it was swimming at higher frequency.

As future work, we aim at to investigate unsteady aquatic propulsion in nature using our Kalman based force-feedback control system. For example, applications that we use self-propelled-control robotic fish to investigate C-start or Burst and Coast motion of living fish. Besides, the centroid oscillation of robotic fish with different kinematics and variable stiffness technology [24] applied in robotic fish will also be research directions for us.

V. CONCLUSION

This paper verified the effectiveness of the self-propelled-control experiment method using ROV and a multi-joint robotic fish. We measured the propulsion velocity of both propeller-based swimmer and fish-like swimmer. We compared the velocity profiles of ROV when it were in FSS and SPCS respectively. The result demonstrates that the velocity profiles measured in FSS and SPCS can basically match the speed under free-swimming states. Moreover, we compared the velocity profiles of two kinds of fish-like swimming locomotion when they are operated under SPCS method. The speed fluctuations that observed on robotic fish are similar to the results from CFD simulations, which suggest that the application of the self-propulsion method in experiments on physical models is promising. Therefore, using our current control system enable constraint-swimming robotic swimmer to simulate free swimming, which can satisfy the self-propulsion conditions and can be used to collect hydrodynamic experimental data. This experimental approach would help us to investigate the principle of unsteady aquatic propulsion in the open water, simply through a tethered robot in lab.

REFERENCES

[1] Sfakiotakis M, Lane D M, Davies J B C. Review of fish swimming modes for aquatic locomotion [J]. IEEE Journal of oceanic engineering, 1999, 24(2): 237-252.

[2] Wang Y, Yang X, Chen Y, et al. A biorobotic adhesive disc for underwater hitchhiking inspired by the remora suckerfish[J]. Science Robotics, 2017, 2(10):eaan8072.

[3] Liang J, Wang T, Wen L. Development of a two‑joint robotic fish for real‑world exploration [J]. Journal of Field Robotics, 2011, 28(1): 70-79.

[4] Yu J, Wang K, Tan M, et al. Design and control of an embedded vision guided robotic fish with multiple control surfaces [J]. The Scientific World Journal, 2014, 2014.

[5] Curet O M, Patankar N A, Lauder G V, et al. Aquatic maneuvering with counter-propagating waves: a novel locomotive strategy [J]. Journal of the Royal Society Interface, 2011, 8(60): 1041-1050.

[6] Kahn Jr J C, Peretz D J, Tangorra J L. Predicting propulsive forces using distributed sensors in a compliant, high DOF, robotic fin [J]. Bioinspiration & biomimetic, 2015, 10(3): 036009.

[7] Beal D N, Bandyopadhyay P R. A harmonic model of hydrodynamic forces produced by a flapping fin [J]. Experiments in Fluids, 2007, 43(5): 675-682.

[8] Esposito C J, Tangorra J L, Flammang B E, et al. A robotic fish caudal fin: effects of stiffness and motor program on locomotor performance [J]. Journal of Experimental Biology, 2012, 215(1): 56-67.

[9] Wu T Y. On theoretical modeling of aquatic and aerial animal locomotion [J]. Advances in applied mechanics, 2002, 38: 291-353.

[10] Wu G, Yang Y, Zeng L. Kinematics, hydrodynamics and energetic advantages of burst-and-coast swimming of koi carps (Cyprinus carpio koi)[J]. Journal of Experimental Biology, 2007, 210(12): 2181-2191.

[11] Tytell E D. Kinematics and hydrodynamics of linear acceleration in eels, Anguilla rostrata[J]. Proceedings of the Royal Society of London B: Biological Sciences, 2004, 271(1557): 2535-2540.

[12] Witt W C, Wen L, Lauder G V. Hydrodynamics of C-start escape responses of fish as studied with simple physical models [J]. Integrative and comparative biology, 2015, 55(4): 728-739.

[13] Feilich K L, Lauder G V. Passive mechanical models of fish caudal fins: effects of shape and stiffness on self-propulsion [J]. Bioinspiration & biomimetic, 2015, 10(3): 036002.

[14] Akanyeti O, Thornycroft P J M, Lauder G V, et al. Fish optimize sensing and respiration during undulatory swimming[J]. Nature communications, 2016, 7: 11044.

[15] Borazjani I. Simulations of unsteady aquatic locomotion: from unsteadiness in straight-line swimming to fast-starts[J]. Integrative and comparative biology, 2015, 55(4): 740-752.

[16] Bottom II R G, Borazjani I, Blevins E L, et al. Hydrodynamics of swimming in stingrays: numerical simulations and the role of the leading-edge vortex[J]. Journal of Fluid Mechanics, 2016, 788: 407-443.

[17] Wen L, Wang T M, Wu G H, et al. Hydrodynamic investigation of a self-propelled robotic fish based on a force-feedback control method[J]. Bioinspiration & biomimetics, 2012, 7(3): 036012.

[18] Wen L, Wang T, Wu G, et al. Quantitative thrust efficiency of a self-propulsive robotic fish: experimental method and hydrodynamic investigation [J]. IEEE/ASME Transactions on Mechatronics, 2013, 18(3): 1027-1038.

[19] Barrett, D., Triantafyllou, M., Yue, et al. Drag reduction in fish-like locomotion. J.Fluid Mech, 1999,392:183-212.

[20] R. E. KALMAN. A New Approach to Linear Filtering and Prediction Problems.Transactions of the ASME–Journal of Basic Engineering, 1960,82:35-45.

[21] Rosario Toscano, Patrick Lyonnet. Robust PID controller tuning based on the heuristic Kalman algorithm. Automatica,2009,45:2099-2106.

[22] L Wen, JC Weaver, GV Lauder. Biomimetic shark skin: design, fabrication and hydrodynamic function[J].Journal of experimental Biology, 2014,217(10):1656-66.

[23] L Wen, JC Weaver, PJ Thornycroft, GV Lauder. Hydrodynamic function of biomimetic shark skin:effect of denticle pattern and spacing [J].Bioinspiration & biomimetics, 2015, 10(6): 066010.

[24] Y Hao, T Wang, L Wen. A Programmable Mechanical freedom and Variable Stiffness Soft Actuator with Low Melting Point Alloy. International Conference in Intelligent Robotics & Apllication, 2017: 151–161.